Atmos. Chem. Phys. Discuss., doi:10.5194/acp-2016-181, 2016
Manuscript under review for journal Atmos. Chem. Phys.
Published: 18 April 2016

Atmospheric Chemistry and Physics
Open Access
Discussions

Validation of OMI Total Column Water Vapor Product

Huiqun Wang[1], Gonzalo Gonzalez Abad[1], Xiong Liu[1], Kelly Chance[1]

[1]Smithsonian Astrophysical Observatory, Cambridge, Massachusetts, 02421, USA

Correspondence to: Huiqun Wang (hwang@cfa.harvard.edu)

Abstract. The Collection 3 Ozone Monitoring Instrument (OMI) Total Column Water Vapor (TCWV) data generated by the Smithsonian Astrophysical Observatory (SAO)'s algorithm Version 1.0.0 and archived at the Aura Validation Data Center (AVDC) are compared with NCAR's ground-based GPS data, AERONET sun-photometer data and Remote Sensing System's SSM/I data. Results show that the OMI data track the seasonal and interannual variability of TCWV for a wide range of climate regimes. During the period from 2005 to 2009, the mean (OMI – GPS) over land is -0.3 mm, the mean (OMI – AERONET) over land is 0 mm, and the mean (OMI – SSM/I) over the ocean is -4.3 mm. The better agreement over land than over the ocean is corroborated by the smaller fitting residuals over land and suggests that liquid water is a key factor for the fitting quality over the ocean in the Version 1.0.0 retrieval algorithm. We find that the influence of liquid water is reduced using a shorter retrieval window. As a result, the TCWV retrieved with the new algorithm increases significantly over the ocean and only slightly over land, improving the land / ocean consistency and the overall quality of whole OMI TCWV dataset.

1 Introduction

Water vapor is an important factor for the weather and climate. It is the most abundant greenhouse gas and can amplify the effect of other greenhouse gasses through positive feedback. It can condense to form clouds that greatly influence the heating rate and circulation of the atmosphere. In addition, it can influence atmospheric composition through photochemical reactions. Water vapor is highly variable in space and time. Better knowledge of its distribution is highly beneficial for predicting the weather, monitoring the climate and understanding the physics and chemistry of the atmosphere.

Water vapor has been observed using a variety of in-situ and remote-sensing techniques. Satellite remote sensing of water vapor has led to products retrieved from the visible (e.g., GOME (Wagner et al., 2003, Lang et al., 2007), SCIAMACHY (Noël et al., 2005), GOME-2 (Grossi et al., 2015), OMI (Wang et al., 2014)), near infrared (e.g., SCIAMACHY (Schrijver et al., 2009), MODIS (Diedrich et al., 2015), MERIS (Lindstrot et al., 2012)), infrared (e.g., MODIS (Seemann et al., 2003), AIRS (Bedka et al., 2010), IASI (Pougatchev et al., 2009)), microwave (e.g., SSM/I(Schlüssel et al., 1990; Wentz, 1997)), and GPS radio signals (e.g., Wang et al., 2007, Kishore et al., 2011). These datasets offer the unique opportunity to study water vapor distribution on a global scale. Among them, microwave and GPS measurements can be made under all-sky conditions. Other types of measurements are strongly affected by clouds. Infrared measurements can provide vertical profiles, but have low sensitivity to the planetary boundary layer where most water vapor resides. Microwave measurements are only available over the non-precipitating ice-free ocean. Near infrared measurements have better quality over land than ocean. Visible measurements are available for both land and ocean but are limited to nearly cloud-free daytime conditions.

Wang et al. (2014) derived Total Column Water Vapor (TCWV, also known as the Total Precipitable Water, TPW) using the spectra measured by the Ozone Monitoring Instrument (OMI). The Level 2 data generated with the Wang et al. (2014) algorithm (Version 1.0.0) for 2005 – 2009 have been archived at the Aura Validation Data Center (AVDC). A detailed assessment of data quality is important for data usage in various weather and climate studies. In this paper, we perform a comprehensive comparison of this product with the ground-based GPS data from NCAR, the near infrared sun-photometer data from AERONET, and the microwave radiometer data from Remote Sensing System (RSS). The various datasets used in this paper will be introduced in Section 2. Comparison results will be presented in Section 3. A modified retrieval algorithm will be presented in Section 4. Conclusions will be drawn in Section 5.

Atmos. Chem. Phys. Discuss., doi:10.5194/acp-2016-181, 2016
Manuscript under review for journal Atmos. Chem. Phys.
Published: 18 April 2016

Atmospheric Chemistry and Physics Discussions

2 Total Column Water Vapor (TCWV) Data

2.1 OMI Data

OMI is an ultraviolet / visible (UV/VIS) imaging spectrometer on board the NASA EOS-Aura satellite. It has three spectral channels spanning the 264 nm – 504 nm spectral region at 0.4 – 0.6 nm spectral resolution (Levelt et al., 2006). OMI has been providing daily global observations at 13:45 LT with a nominal spatial resolution of 13 km × 24 km at nadir since July 2004.

Water vapor exhibits several distinct spectral bands in the OMI visible channel (349 nm – 504 nm). These features are several orders of magnitude weaker than those at longer wavelengths. However, they can still be exploited to retrieve TCWV (Wagner et al., 2013; Wang et al., 2014). Since water vapor is a weak absorber in the blue spectral range, the retrieval is free from the complication of non-linearity due to saturation. Since the surface albedo is more uniform over the globe in this spectral region, the signals do not change abruptly between land and ocean. Water vapor derived from the blue spectral range can greatly enhance the scientific return of satellites, especially for those with instruments that lack spectral coverage at longer wavelengths (e.g., OMI).

Wang et al. (2014) retrieved TCWV from OMI spectra in the 430 nm – 480 nm retrieval window using a two-step method. First, the Slant Column Density (SCD) is derived from a spectral fitting that considers water vapor, O_3, NO_2, O_2-O_2, $C_2H_2O_2$, liquid water, the Ring effect, the water Ring effect, 3rd order closure polynomials, wavelength shift, under-sampling and common mode. The median SCD fitting error is about 11% (Wang et al., 2014). Then, the Vertical Column Density (VCD) is obtained by dividing the SCD with an Air Mass Factor (AMF) that is based on a radiative transfer calculation. Wang et al. (2014) found that the AMF was insensitive to wavelength, but sensitive to surface albedo and highly sensitive to clouds. The VCD in molecules / cm^2 can be converted to TCWV in mm using a multiplicative factor of 2.989×10^{-22}. The Collection 3 Version 1.0.0 Level 2 OMI water vapor VCD data from 2005 to 2009 have been released at the AVDC website (avdc.gsfc.nasa.gov). These data will be validated in this paper.

It should be noted that there are artificial stripes in the Level 2 OMI water vapor data. These stripes are due to systematic errors related to instrument calibration. They can be smoothed by post-processing the Level 2 data. One smoothing method is to divide the SCD with a one-dimensional (1D) smoothing array whose mean is normalized to unity (Wang et al., 2014). As an example, Figure 1 shows the smoothing array as a function of pixel number (one for each month of 2005). Each array is calculated from the multi-line mean of a month of Level 2 SCD swaths

Atmos. Chem. Phys. Discuss., doi:10.5194/acp-2016-181, 2016
Manuscript under review for journal Atmos. Chem. Phys.
Published: 18 April 2016

Atmospheric Chemistry and Physics
Discussions
Open Access

and normalized by a 3rd order polynomial fit (as a function of pixel number). Figure 1 shows large pixel-to-pixel variations with cross-track standard deviations in the range of 12% - 30%. Consequently, the stripes can significantly influence the day-to-day comparisons between the Level 2 OMI data and other datasets. Another smoothing method is to subtract a 1D offset array from the SCD before the SCD is converted to VCD. The offset array can be derived from a reference region, such as the Sahara. For each swath to be de-striped, the mean SCD of each cross-track pixel is calculated for the reference region using the swaths within a week, a low-order (e.g., third order) polynomial is removed, and the resulting 1D array is used as the offset array. Since the smoothing procedure is non-unique and can potentially introduce additional bias, we use the un-smoothed Level 2 TCWV data (with stripes) in this paper.

2.2 NCAR Ground-based GPS Data

NCAR hosts a 2-hourly TCWV dataset derived from the ground-based GPS measurements of Zenith Path Delay (ZPD) at stations in the International GNSS Service (IGS), SuomiNet, and GEONET networks (Wang et al., 2007). We have downloaded the data from rda.ucar.edu/datasets/ds721.1/ (EOL/NCAR/UCAR, 2011, updated yearly). The IGS- SuomiNet data include 1160 stations worldwide and are available from 1995 to 2012. The ground-based GPS data have been extensively used to validate other TCWV measurements and data assimilation products (Wang and Zhang, 2008, Sibelle et al., 2010, Mears et al., 2015). The GPS TCWV retrieval error is estimated to be 1.5 mm (Wang et al., 2007). The mean difference between the GPS and satellite microwave radiometer data over the ocean is < 1 mm and the standard deviation is < 2 mm (Mears et al., 2015). In this paper, we use the subset of IGS-SuomiNet data from 2005 to 2009 to compare with the OMI data.

2.3 AERONET Sun-photometer Data

The AErosol RObotic Network (AERONET) provides globally distributed observations of aerosol optical depth, TCWV, and other variables using sun-photometers (Holben et al., 1998). The network has expanded from 16 sites in 1993 to 860 sites in 2014. The TCWV is derived from the 940 nm filter that coincides with the $2\nu_1+\nu_2$ water vapor absorption band. The Level 2.0 AERONET data are cloud screened and quality assured (Smirnov et al., 2000). We have downloaded the publically available Version 2 Level 2.0 data from aeronet.gsfc.nasa.gov and used the subset from 2005 to 2009 to compare with the OMI Level 2 data. Using the subset of AERONET data observed at the sites operated by U.S. Department of Energy Atmospheric Radiation Measurement (ARM) program, Pérez-Ramírez et al. (2014) found that the AERONET TCWV had a general dry bias of 5 – 6% and an estimated uncertainty of 12 – 15%. The Version 3 AERONET data is currently in development and is expected to be released in 2016.

Atmos. Chem. Phys. Discuss., doi:10.5194/acp-2016-181, 2016
Manuscript under review for journal Atmos. Chem. Phys.
Published: 18 April 2016

Atmospheric Chemistry and Physics Discussions

2.4 RSS SSM/I Microwave Radiometer Data

The Remote Sensing Systems (RSS) generates TCWV data by processing the microwave radiometer data from Special Sensor Microwave / Imager (SSM/I), Special Sensor Microwave Imager Sounder (SSMIS), and other sensors. Their retrieval uses a unified physically based algorithm (Wentz, 1997). The TCWV data derived from these satellite microwave radiometers are available under all-sky non-precipitating conditions over the ice-free ocean. They have long been considered as among the most reliable and have been routinely assimilated into numerical models. We have downloaded the latest Version 7 SSM/I F16 data from www.remss.com (Wentz et al., 2012). Abnormal conditions (heavy rain, sea ice, bad data, no observation, and land) are flagged in these data. In this paper, we use both the monthly and daily gridded (0.25° × 0.25°) data from 2005 to 2009.

3 Comparison Results

3.1 OMI and GPS

The AVDC Collection 3 Version 1.0.0 Level 2 OMI data are filtered and co-located with NCAR's ground-based GPS data. The filtering criteria for OMI require that the general quality check is passed (Main_Data_Quality_Flag MDQF = 0), the SCD fitting Root Mean Square (RMS) is $< 10^{-3}$, the cloud fraction is < 10%, the cloud top pressure is > 500 hPa, and the AMF is > 0.75. Since clouds can dramatically change the vertical sensitivities and lead to large errors in OMI retrievals (Wang et al., 2014), the last three criteria are intended to mitigate their influence. For co-location at each GPS station, we select the GPS observations made between the local noon and 14:00 LT each day. For each eligible GPS data point, we search the filtered OMI data on the same day for the pixels that are within 0.25° latitude × 0.25° longitude of the GPS station. If multiple OMI data points are found for a single GPS data point, then the average weighted by the fitting error is calculated and used for the comparison.

Figure 2 shows the TCWV time series comparison between the GPS and OMI data at selected sites. These sites are scattered around the world (denoted by "X" in Figure 3) and represent a variety of climate regimes. For both dry and wet conditions and for both small and large seasonal cycles, the OMI data track the seasonal and inter-annual variations of the GPS data well, even with the influence of stripes.

The top panel of Figure 3 shows the (OMI – GPS) TCWV difference averaged within the time period from January 1, 2005, to December 31, 2009, for the IGS-SuomiNet stations. For this plot, we have excluded the stations with significant topography difference (i.e. those with elevations that are different than the local gridded (0.25°×0.25°) topography by 500 m or more).

We have also excluded the stations with < 100 data points. There are 250 stations in Figure 3. Many are in North America and Europe, but very few are in Africa and on ocean islands. Generally speaking, OMI data agree well with GPS data over land but are significantly lower over the ocean. The histogram for the mean (OMI – GPS) TCWV difference is plotted in the bottom panel of Figure 3. It is binned by 0.5 mm and has a mode of -0.5 mm. OMI data agree with GPS data within 1.5 mm at 71% of the stations and within 3 mm at 89% of the stations. OMI data are higher than GPS data by 3 mm or more at 8 stations, where all except for one station are located in coastal areas. OMI data are lower than GPS data by 3 mm or more at 23 stations, where all except for 2 stations are located on ocean islands or in coastal areas. OMI data are lower than GPS data by 5 mm or more at 10 stations, among which, 2 stations are located in coastal areas and the others are on ocean islands.

In Figure 4, we compare OMI with GPS TCWV using all available data pairs at all land (left) and ocean (right) stations without significant topography difference. Since most GPS stations are over land, the number of data points over land (317,118) far exceeds that over the ocean (2,621). The top row shows the 2D histogram of GPS versus OMI TCWV. The data are binned every 0.5 mm. The largest color-coded value in each panel is normalized to one. The GPS TCWV data over land are mostly within the (10% - 90% percentile) range of 4 – 34 mm and those over the ocean are mostly within 17 – 50 mm. The OMI data generally follow the GPS data along the 1:1 line over land, but tend to be lower than the GPS data (i.e., below the 1:1 line) over the ocean. The bottom row shows the histograms for the (OMI – GPS) differences. The histogram for land stations has a peak at 0 mm. The distribution is slightly asymmetric, with a Full-Width-at-Half-Maximum (FWHM) of 8.5 mm (from -5.0 mm to 3.5 mm). The mean and median of the distribution are -0.3 mm and -0.4 mm, respectively. The scatter is related to random errors in GPS data and random errors in OMI SCD, AMF, and stripes. The histogram for the ocean stations is much less smooth due to the smaller sample size. The distribution is apparently skewed towards more negative values and has a larger scatter. The mode, mean, and median of OMI – GPS over the ocean are -1.5 mm, -3 mm, and -3.5 mm, respectively.

3.2 OMI and AERONET

We filter and co-locate OMI and AERONET TCWV data following the same procedure as that in Section 3.1. Figure 5 shows time series comparisons at selected AERONET sites. These sites represent a wide range of water vapor amounts and seasonal cycles around the world (denoted by “X” in Figure 6). In general, OMI observations track the variations of AERONET data well. During the wet season, OMI data appear to be higher at several sites (e.g., Skukuza, Mukdahan, GSFC, Hamburg, and Dakar).

Atmos. Chem. Phys. Discuss., doi:10.5194/acp-2016-181, 2016
Manuscript under review for journal Atmos. Chem. Phys.
Published: 18 April 2016

In Figure 6, we examine the spatial distribution and histogram of the mean of (OMI – AERONET) for the time period from 2005 to 2009. As in Figure 3, we have omitted the sites with substantial topography difference and the sites with < 100 data points. Figure 6 shows that OMI is generally higher over land and lower over the ocean and in some coastal areas. The histogram shows a main peak at 0.5 mm and a secondary peak at -2.5 mm. The secondary peak is due to the ocean sites. 59% of the sites show a non-negative OMI – AERONET difference. Pérez-Ramírez et al. (2014) found a dry bias of AERONET TCWV at the US Southern Great Plains, Barrow (in Alaska) and Nauru islands (in the tropical western Pacific). Figure 6 suggests that OMI is slightly wetter than AERONET in the contiguous US and Alaska, but is even drier than AERONET at Nauru island.

In Figure 7, we compare OMI with AERONET TCWV using all data pairs from 2005 to 2009 at all land (left) and ocean (right) sites that are without significant topography. The top row shows the 2D normalized histograms for AERONET versus OMI data and the bottom row shows the histograms for the (OMI – AERONET) differences. Both are calculated using a 0.5 mm bin. There are far more data points over land (91,350) than over the ocean (3,092). TCWV over the ocean is generally larger than that over land. The 10% and 90% percentiles of AERONET data for the ocean sites are 13 mm and 45 mm, while those for the land sites are 6 mm and 32 mm. Figure 7 shows that OMI agrees with AERONET well over land, but tends to be lower than AERONET over the ocean. The (OMI-AERONET) histogram for the land sites has a peak of -1 mm and an FWHM of 8.5 mm (from -5.0 mm to 3.5 mm), while that for the ocean sites has a peak of -3.5 mm and an FWHM of 12 mm (from -9.5 mm to 2.5 mm). The mean and median of (OMI – AERONET) over land are 0 mm and -0.3 mm, respectively, and those over the ocean are -2.0 mm and -2.6 mm, respectively.

3.3 OMI and SSM/I

The SSM/I TCWV data from RSS are specifically for the ocean and have a long-term daily coverage. We therefore use them to evaluate our OMI product over the ocean. In Figure 8, we compare the monthly mean OMI data (top row) with the monthly mean RSS data (middle row) for July 2005. The Level 3 monthly OMI data are gridded at 0.25°×0.25° resolution from the corresponding Level 2 data using the average weighted by the area and slant column fitting uncertainty (Wang et al., 2014). Note that the stripes in the Level 2 OMI data are averaged out in the monthly Level 3 product. The selection criteria for gridding the OMI Level 2 data include MDQF = 0, AMF > 0.75, cloud top pressure > 500 mb, and cloud fraction < a cutoff value.

To compare with the all-sky monthly mean SSM/I data (middle left panel), the OMI Level 2 data are gridded with a relaxed cloud fraction cutoff of 25% (top left panel). It can be seen that OMI captures the general spatial distribution of TCWV observed by SSM/I. However, OMI data

Atmos. Chem. Phys. Discuss., doi:10.5194/acp-2016-181, 2016
Manuscript under review for journal Atmos. Chem. Phys.
Published: 18 April 2016

Atmospheric Chemistry and Physics Discussions
Open Access

tend to be lower. The (OMI – SSM/I) difference has a global mean of -4.3 mm and can be < -10 mm in the Western Pacific. The difference between OMI and SSM/I is smaller when a larger cloud fraction cutoff is used, and vice versa. For example, for a 50% cloud fraction cutoff, the global mean of (OMI – SSM/I) becomes -3.4 mm. However, the OMI data quality is generally lower for cloudier scene as the AMF is highly sensitive to clouds.

In the right column of Figure 8, we compare the monthly mean SSM/I and OMI data under "clear" sky conditions for July 2005. The monthly mean OMI data in the top right panel are gridded using a stricter cloud fraction cutoff of 5%. This choice is based on a balance between the cloudiness and the number of data points available for each grid box. The monthly mean SSM/I data in the middle right panel are calculated by averaging the daily SSM/I gridded data and ignoring the pixels whose cloud liquid water path is > 0. Both the SSM/I (middle row) and the OMI (top row) data show a decrease in TCWV as the cloud amount decreases. However, compared with the bottom left panel, OMI – SSM/I in the bottom right panel shows even larger negative values. In fact, the global mean of (OMI – SSM/I) becomes -5.9 mm and most of the northern tropical ocean areas now show values that are < -10 mm.

Figure 9 shows the 2D normalized histogram of OMI versus SSM/I data for July 2007. The histograms are calculated using the daily gridded (0.25°×0.25°) SSM/I and OMI data. The same data filtering criteria as before are applied except for an OMI cloud fraction cutoff of 10%. This cutoff value is between the 5% and 25% used in Figure 8. We compare the OMI data with the SSM/I "clear" sky data in the top left panel and all-sky data in the top right panel. Both show that OMI is lower than SSM/I. The mean (OMI – SSM/I) difference for the all-sky case (-4.4 mm) is a little larger than that for "clear" sky case (-3.7 mm). The standard deviation of (OMI – SSM/I) is 7.7 mm for the all-sky case and 7.2 mm for the "clear" sky case.

4 Algorithm Update

The previous section shows that the AVDC Collection 3 Version 1.0.0 OMI data agree well with the GPS and sun-photometer observations over land but have a low bias over the ocean. Wang et al. (2014) showed that liquid water is an important molecule to consider in their retrieval algorithm. They also showed that the fitting residual is generally larger over the ocean than over land, the common mode derived over land appears largely random but that derived over the ocean has apparent spectral structures, especially between 440 nm and 470 nm where the liquid water reference spectrum exhibits distinct spectral features (Pope and Fry, 1997). Consequently, errors in liquid water spectroscopy can lead to systematic errors in water vapor retrieved over the ocean. Furthermore, the 430 – 480 nm retrieval window used by Wang et al. contains the 7ν (435 – 450 nm) and $6\nu+\delta$ (460 – 480 nm) spectral bands of water vapor. Lampel et al. (2015) derived scaling factors for the water vapor absorption bands in the blue spectral

Atmos. Chem. Phys. Discuss., doi:10.5194/acp-2016-181, 2016
Manuscript under review for journal Atmos. Chem. Phys.
Published: 18 April 2016

range using the 7ν band as a reference. They suggested that the absorption strength of the 6ν+δ band should be scaled by 1.02±0.07 in HITRAN 2008 (Rothman et al., 2009), which would affect water vapor retrieval derived from the 430 – 480 nm window.

To reduce the influence of errors in liquid water and water vapor cross sections, we experimented with retrievals using a narrower retrieval window. We derived the 427.7 – 465.0 nm retrieval window by optimizing around the 7ν water vapor band in OMI spectra. In addition, since water vapor over the ocean is more concentrated at the sea level, we changed the HITRAN 2008 water vapor reference spectra from one that corresponds to 0.9 atm and 280K to one that corresponds to 1.0 atm and 288K. We have recently obtained the O_2-O_2 spectra measured by Thalman and Volkamer (2013) at 0.82 mb and 293K. We therefore also updated the O_2-O_2 reference spectra in our new algorithm. All the other retrieval setups remain the same as those used in the AVDC Collection 3 algorithm Version 1.0.0 (Wang et al., 2014). The differences in TCWV between this algorithm and the Version 1.0.0 algorithm mainly come from the change in the retrieval window. As shown in Wang et al. (2014), the fitting uncertainty for shorter retrieval window is larger. For example, the median absolute uncertainty for July 14, 2005 increases from 1.05×10^{22} molecules / cm^2 in Version 1.0.0 to 1.35×10^{22} molecules / cm^2 in this new version. However, the relative uncertainty remains at 12% for both. As will be shown next, the monthly mean values derived from the new retrieval algorithm lead to a better agreement with the SSM/I data.

Using the new setup described above, we retrieved the Level 2 TCWV for July 2005 and generated daily 0.25°×0.25° Level 3 TCWV using the same filtering criteria as before. In the bottom row of Figure 9, we compare the new OMI daily gridded data (with a 10% cloud fraction cutoff) with the SSM/I "clear" sky (bottom left) and all-sky (bottom right) daily gridded data over the ocean. Results show a much better agreement between the new OMI and SSM/I data. The mean and median of (new OMI – SSM/I) is now 1.3 mm and 0.8 mm for "clear" sky condition and 0.6 mm and 0.1 mm for all-sky condition, indicating a significant improvement of the new OMI retrieval over the ocean.

To investigate the spatial distribution of the changes between the AVDC Collection 3 data and new OMI retrievals, we compare the monthly mean Level 3 gridded (0.25°×0.25°) data. The top row of Figure 10 shows the (new OMI – AVDC OMI) difference maps for a 5% (right) and a 25% (left) cloud fraction cutoff. In both cases, the new OMI data increase a little over land but increase substantially over the ocean. For the 5% cloud fraction cutoff, the new OMI data increase over the AVDC OMI data by an average of 1.2 mm over land and 4.8 mm over the ocean. For the 25% cutoff, the new OMI data increase by an average of 1.3 mm over land and 3.7 mm over the ocean.

We compare the gridded monthly mean new OMI data with the RSS SSM/I data in the bottom row of Figure 10. The bottom right panel shows the difference of (new OMI with a 5% cloud fraction cutoff – "clear" sky SSM/I). The global mean of this value over the ocean is -0.68 mm. The bottom left panel shows the difference of (New OMI with a 25% cutoff – all-sky SSM/I). The global mean over the ocean is -0.23 mm. The large positive values (> 6 mm) in the lower left all-sky case are due to the presence of clouds. In comparison with the bottom row of Figure 8, there is apparently a significantly improved agreement when the new OMI retrieval algorithm is used.

5 Summary

The AVDC Collection 3 OMI TCWV data generated with algorithm Version 1.0.0 are compared with the NCAR's ground-based GPS network observations, AERONET sun-photometer observations and RSS's SSM/I microwave radiometer observations. Results show that the AVDC OMI data track the seasonal and interannual variability of TCWV for a wide range of climate regimes. The OMI data agree well with other data sets over land, but show quite large low biases over the ocean. For co-located data from January 2005 to December 2009, (OMI – GPS) over land has a mean of -0.3 mm and a median of -0.4mm, and (OMI – AERONET) over land has a mean of 0 mm and a median of -0.3 mm. In comparison, OMI data (with cloud fraction < 10%) are lower than SSM/I all-sky data over the ocean by an average of 4.4 mm.

By reducing the retrieval window length from 430-480 nm to 427.5 – 465.0 nm, using water vapor reference spectra at the sea level, and incorporating a new O_2-O_2 reference spectrum, the new algorithm can significantly increase the retrieved TCWV over the ocean without affecting those over land much, leading to better agreements with other datasets. For July 2005, the new OMI data (with cloud fraction < 10%) are on average 0.6 mm higher than the SSM/I all-sky data and 1.3 mm higher than the SSM/I "clear" sky data. This update will be considered in the next release of SAO's OMI water vapor product.

Acknowledgement

This paper is supported by NASA's Atmospheric Composition: Aura Science Team program (Sponsor Contract Number NNX14AF56G). We thank NASA's Aura Validation Data Center (avdc.gsfc.nasa.gov) for generating and archiving OMI water vapor product. The GPS precipitable water data are downloaded from rda.ucar.edu/datasets/ds721.1. The AERONET Version 2 total column water vapor data are downloaded from aeronet.gsfc.nasa.gov/new_web/data.html. The SSM/I and SSMIS data are produced by Remote

Sensing Systems (RSS) and sponsored by the NASA Earth Science MEaSUREs Program and are available at www.remss.com.

References

Bedka, S., Knuteson, R., Revercomb, H., Tobin, D., and Turner, D.: An assessment of the absolute accuracy of the Atmospheric Infrared Sounder v5 precipitable water vapor product at tropical, midlatitude, and arctic ground-truth sites: September 2002 through August 2008, J. Geophys. Res., 115, doi:10.1029/2009JD013139, 2010.

Grossi, M., Valks, P., Loyola, D., Aberle, B., Slijkhuis, S., Wagner, T., Beirle, S., and Lang, R.: Total column water vapour measurements from GOME-2 MetOP-A and MetOP-B, Atmos. Meas. Tech., 8, 1111-1133, doi:10.5194/amt-8-1111-2015, 2015.

Earth Observing Laboratory/National Center for Atmospheric Research/University Corporation for Atmospheric Research, 2011, updated yearly. NCAR Global, 2-hourly Ground-Based GPS Precipitable Water. Research Data Archive at the National Center for Atmospheric Research, Computational and Information Systems Laboratory. http://rda.ucar.edu/datasets/ds721.1/. Accessed December 2015.

Holben, B.N., Eck, T.F., Slutsker, I., Tanre, D., Buis, J.P., Setzer, A., Vermote, E., Reagan, J.A., Kaufman, Y.J., Nakajima, T., Lavenu, F., Jankowiak, I., Smirnov, A.: AERONET – A federated instrument network and data archive for aerosol characterization, Remote Sensing of Environment, 66, 1 – 16, doi:10.1016/S0034-4257(98)00031-5, 1998.

Kishore, P., Ratnam, M.V., Namboothiri, S.P., Velicogna, I., Basha, G., Jiang, J.H., Igarashi, K., Rao, S.V.B., Sivakumar, V.: Global (50 degrees S – 50 degrees N) distribution of water vapor observed by COSMIC GPS RO: Comparison with GPS radiosonde, NCEP, ERA-Interim, and JRA-25, J, Atmospheric & Solar –Terrestrial Phys., 73, 1849-1860, 2011.

Lang, R., Casadio, S., Maurellis, A.N., and Lawrence, M.G.: Evaluation of the GOME water vapor climatology 1995-2002, JGR, doi:10.1029/2006JD008246, 2007.

Levelt, P.F., van den Oord, G.H.J., Dobber, M.R., Malkki, A., Visser, H., de Vries, J., Stammes, P., Lundell, J.O.V., and Saari, H.: The Ozone Monitoring Instrument, IEEE T. Geosci. Remote, 44, 1093-1101, 2006.

Lindstrot, R., Preusker, R., Diedrich, H., Doppler, L., Bennartz, R., and Fischer, J.: 1D-Var retrieval of daytime total column water vapour from MERIS measurements, Atmos. Meas. Tech., 5, 631-646, doi:10.5194/amt-5-631-2012, 2012.

Atmos. Chem. Phys. Discuss., doi:10.5194/acp-2016-181, 2016
Manuscript under review for journal Atmos. Chem. Phys.
Published: 18 April 2016

Atmospheric Chemistry and Physics Discussions

Mears, C., Wang, J., Smith, D., and Wentz, F.: Intercomparison of total precipitable water measurements made by satellite-borne microwave radiometers and ground-based GPS instruments, J. Geophys. Res. Atmos., 120, 2492-2504, doi:10.1002/2014JD022694, 2015.

Noël, S., Buchwitz, M., Bovensmann, H., and Burrows, J.P.: Validation of SCIAMACHY AMC-DOAS water vapour columns, Atmos. Chem. Phys., 5, 1835-1841, doi:10.5194/acp-5-1835-2005, 2005.

Pérez-Ramírez, D., Whiteman, D.N., Smirnov, A., Lyamani, H., Holben, B.N., Pinker, R., Andrade, M., and Alados-Arboledas, L.: Evaluation of AERONET precipitable water vapor versus microwave radiometry, GPS, and radiosondes at ARM sites, J. Geophys. Res. Atmos., 119, 9596-9613, doi:10.1002/2014JD021730, 2014.

Pougatchev, N., August, T., Calbet, X., Hultberg, T., Oduleye, O., Schüssel, P., Stiller, B., Germain, K. St., and Bingham, G.: IASI temperature and water vapor retrievals – error assessment and validation, Atmos. Chem. Phys., 9, 6453-6458, doi:10.5194/acp-9-6453-2009, 2009.

Pope, R.M. and Fry, E.S.: Absorption spectrum (380 – 700 nm) of pure water. 2. Integrating cavity measurements, Appl. Optics, 36, 8710-8723, doi:10.1364/AO.36.008710, 1997.

Rothman, L. S., Gordon, I. E., Barbe, A., Benner, D. C., Bernath, P. F., Birk, M., Boudon, V., Brown, L. R., Campargue, A., Champion, J.-P., Chance, K., Coudert, L. H., Dana, V., Devi, V. M., Fally, S., Flaud, J. M., Gamache, R. R., Goldman, A., Jacquemart, D., Lacome, N., Lafferty, W. J., Mandin, J. Y., Massie, S. T., Mikhailenko, S. N., Miller, C. E., Moazzen-Ahmadi, N., Naumenko, O. V., Nikitin, A. V., Orphal, J., Perevalov, V. I., Perrin, A., Predoi-Cross, A., Rinsland, C. P., Rotger, M., Simeckova, M., Smith, M. A. H., Sung, K., Tashkun, S. A., Tennyson, J., Toth, R. A., Vandaele, A. C., and Vander Auwera, J.: The HITRAN 2008 molecular spectroscopic database, J. Quant. Spectr. Radiat. Tran., 110, 533–572, 2009.

Seemann, S.W., Menzel, W.P. and Gumley, L.E.: Operational retrieval of atmospheric temperature, moister, ad ozone from MODIS infrared radiances, J. Applied Meteorology, 42, 8, 1072-1091, doi:10.1175/1520-0450(2003)042<1072:OROATM>2.0.CO;2, 2003.

Schlüssel, P. and Emery, W.J.: Atmospheric water vapour over oceans from SSM/I measurements, Int. J. Remote Sen., 11, 753-766, doi:10.1080/01431169008955055, 1990.

Schrijver, H. Gloudemans, A.M.S., Frankenberg, C., and Aben, I.: Water vapour total columns from SCIAMACHY spectra in the 2.36 µm eindow, Atmos. Meas. Tech., 2, 561-571, doi:10.5194/amt-2-561-2009, 2009.

Atmos. Chem. Phys. Discuss., doi:10.5194/acp-2016-181, 2016
Manuscript under review for journal Atmos. Chem. Phys.
Published: 18 April 2016

Atmospheric Chemistry and Physics
Discussions

Sibylle, V., Dietrich, R., Rülke, A., and Fritsche, M.: Validation of precipitable water vapor within the NCEP/DOE reanalysis using global GPS observations from one decade, J. Climate, 23, 1675-1695, doi:10.1175/2009JCLI2787.1, 2010.

Smirnov, A., Holben, B.N., Eck, T.F., Dubovik, O., and Slutsker, I.: Cloud-screening and quality control algorithms for the AERONET database, Remote Sensing of Environment, 73, 337-349, doi:10.1016/S0034-4257(00)00109-7, 2000.

Thalman, R. and Volkamer, R., 2013. Temperature dependent absorption cross-sections of O-2-O-2 collision pairs between 340 and 630 nm and at atmospherically relevant pressure. Physical Chemistry Chemical Physics, 15, 37, 15371-15381, doi:10.1039/c3cp50968k.

Wagner, T., Heland, J., Zöger, M., and Platt, U.: A fast H2O total column density product from GOME – Validation with in-situ aircraft measurements, Atmos. Chem. Phys., 3, 651-663, www.atmos-chem-phys.org/acp/3/651, 2003.

Wagner, T., Beirle, S., and Mies, K.: A feasibility study for the retrieval of the total column precipitable water vapour from satellite observations in the blue spectral range, Atmos. Meas. Tech., 6, 2593-2605, doiL10.5194/amt-6-2593-2013, 2013.

Wang, J., Zhang, L., Dai, A., Van Hove, T., and Van Baelen, J.: A near-global, 2-hourly data set of atmospheric precipitable water from ground-based GPS measurements, J. Geophys. Res., 112, D11107, doi/l10.1029/2006JD007529, 2007.

Wang, J. and Zhang, L.: Systematic errors in global radiosonde precipitable water data from comparisons with ground-based GPS measurements, J. Climate, 21, 2218-2238, doi:10.1175/2007JCLI944.1, 2008.

Wang, H., Liu, X., Chance, K., González Abad, G., and Chan Miller, C.: Water vapor retrieval from OMI visible spectra, Atmos. Meas. Tech., 7, 1901-1913, doi:10.5194/amt-7-1901-2014, 2014.

Wentz, F.J.: A well-calibrated ocean algorithm for special sensor microwave / imager, J. Geophys. Res., 102, 8703-8718, 1997.

Wentz, F.J., Hilburn, K.A., Smith, D.K., 2012: Remote Sensing Systems DMSP SSM/I Daily and Monthly Environmental Suite on 0.25 deg grid, Version 7. Remote Sensing Systems, Santa Rosa, CA. Available online at www.remss.com/missions/ssmi. Accessed December 2015.

Atmos. Chem. Phys. Discuss., doi:10.5194/acp-2016-181, 2016
Manuscript under review for journal Atmos. Chem. Phys.
Published: 18 April 2016

Atmospheric Chemistry and Physics
Open Access
Discussions

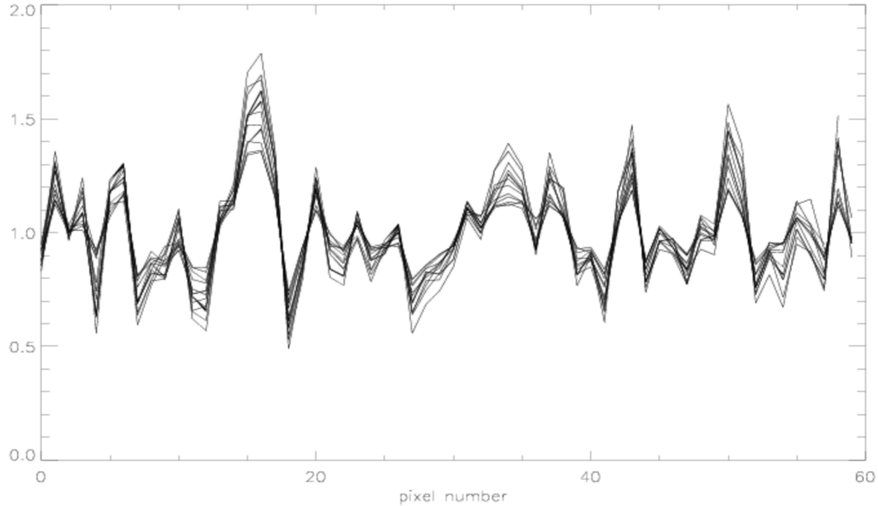

Figure 1. Stripes in TCWV for each month of 2005. The mean of each curve is normalized to 1.

425

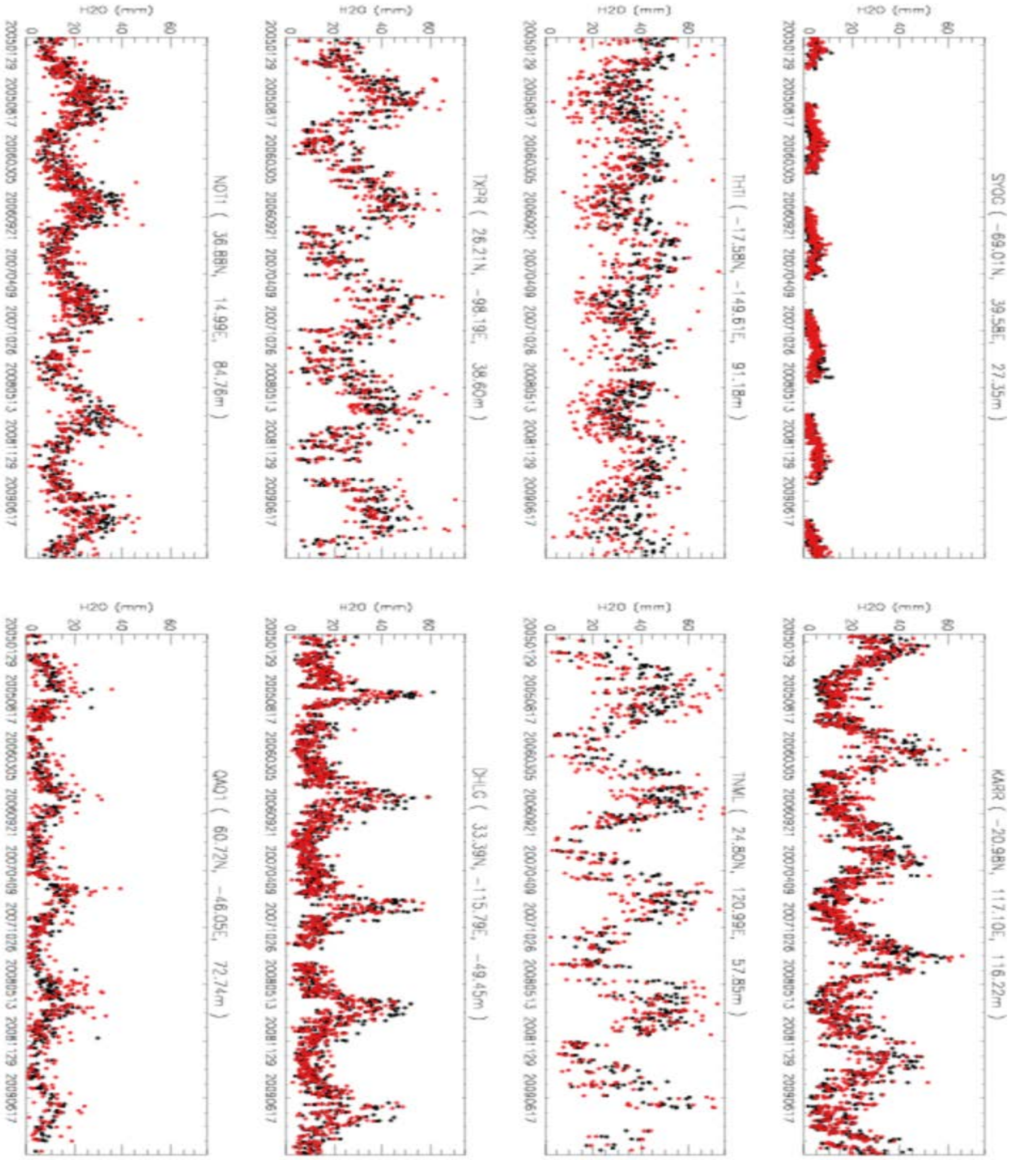

426

427 **Figure 2.** Time series comparison between OMI (red) and GPS (black) at selected stations from
428 January 1, 2005, to December 31, 2009.

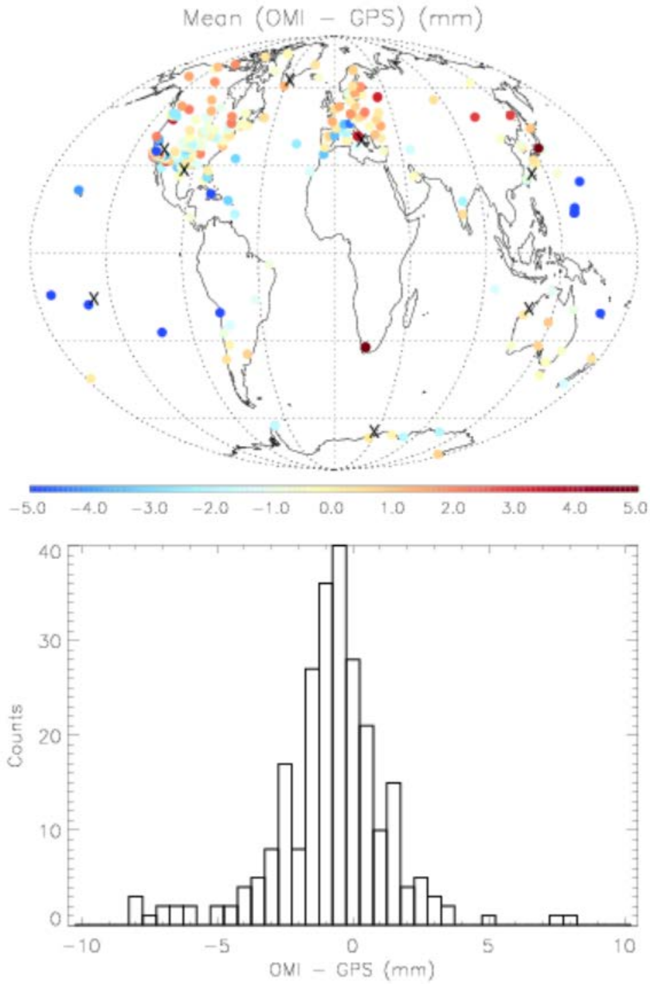

Figure 3. (Top) Spatial distribution of the mean of (OMI – GPS) from 2005 to 2009 at IGS-SuomiNet stations. (Bottom) Histogram (with a 0.5 mm bin size) for the values in the top panel.

Atmos. Chem. Phys. Discuss., doi:10.5194/acp-2016-181, 2016
Manuscript under review for journal Atmos. Chem. Phys.
Published: 18 April 2016

Atmospheric Chemistry and Physics Discussions

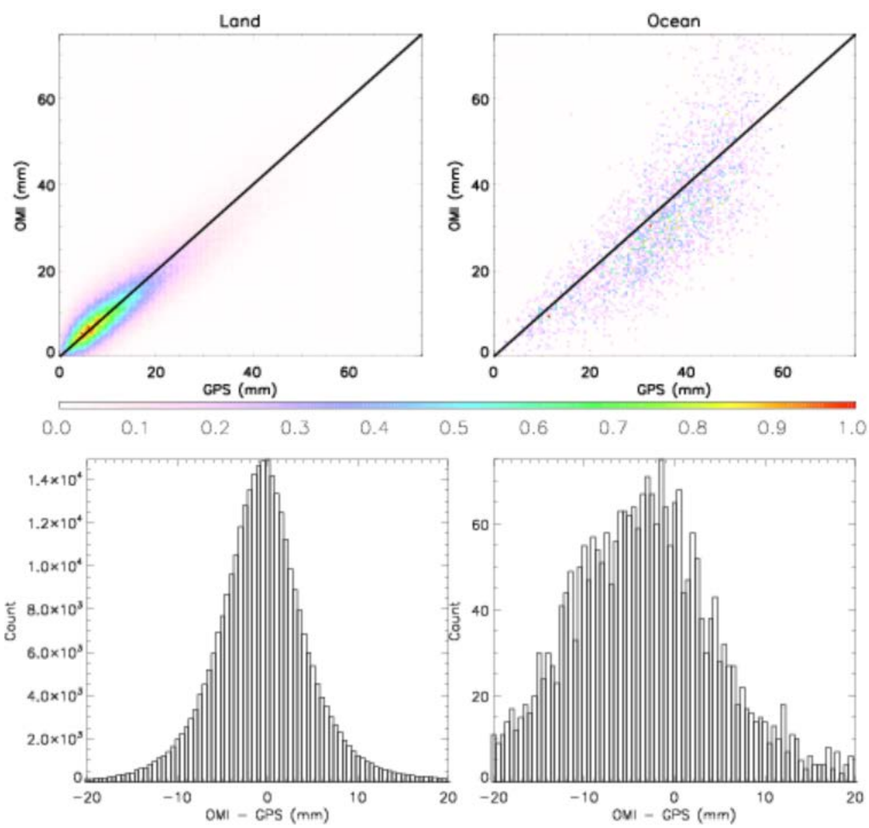

Figure 4. (Top) 2D normalized histogram for (left) land and (ocean) derived from all the paired OMI and GPS data at all suitable IGS-SuomiNet stations from January 1, 2005 to December 31, 2009. Results are shown for 0.5 mm × 0.5 mm bins, with the largest binned value normalized to 1. The black line in each panel corresponds to 1:1. (Bottom) Histogram of (OMI – GPS) derived from the same data as those used in the top panel. The counts correspond to 0.5 mm bins.

Atmos. Chem. Phys. Discuss., doi:10.5194/acp-2016-181, 2016
Manuscript under review for journal Atmos. Chem. Phys.
Published: 18 April 2016

Atmospheric Chemistry and Physics
Discussions

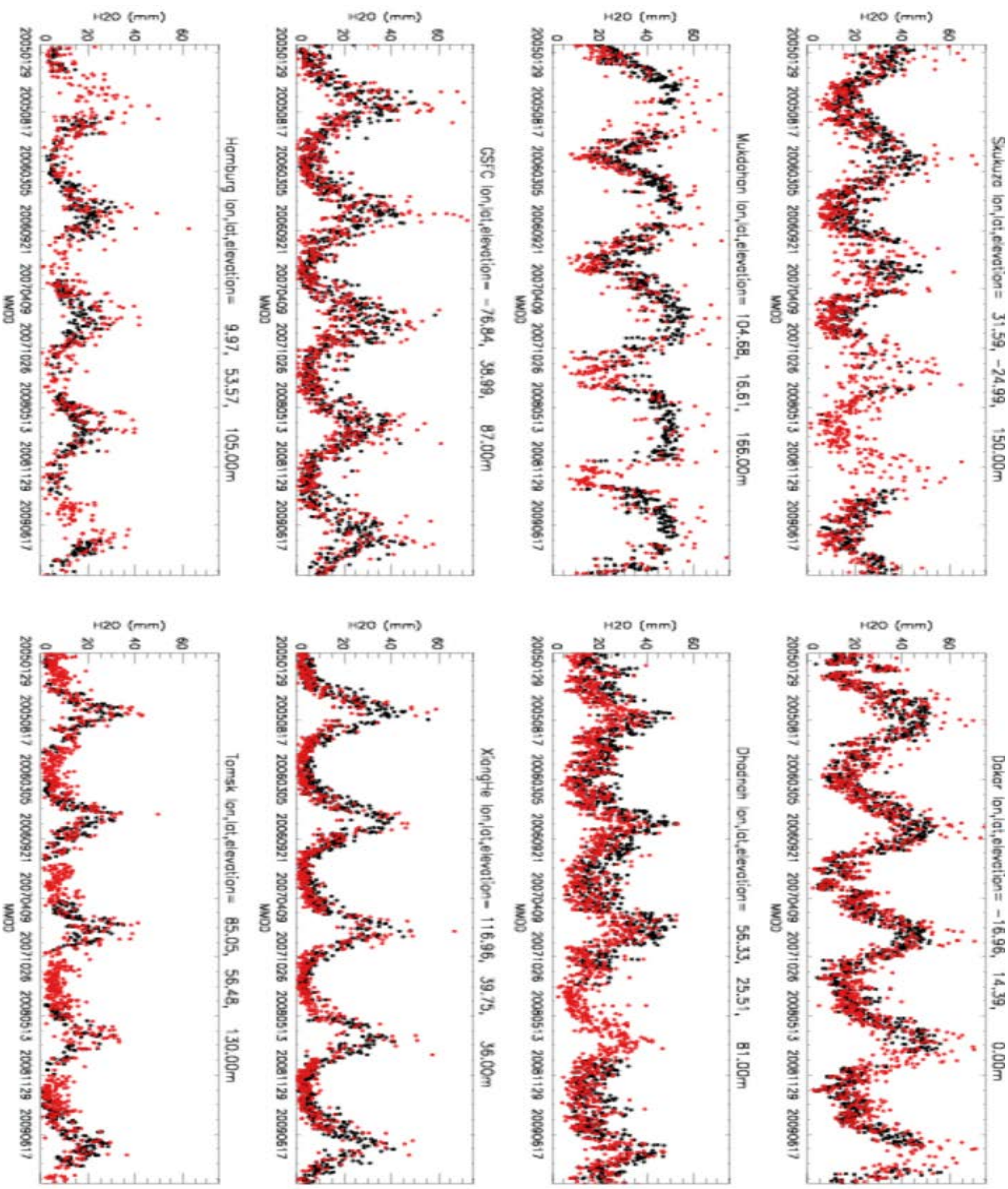

Figure 5. Time series comparison between OMI (red) and AERONET (black) at selected AERONET stations from January 1, 2005, to December 31, 2009.

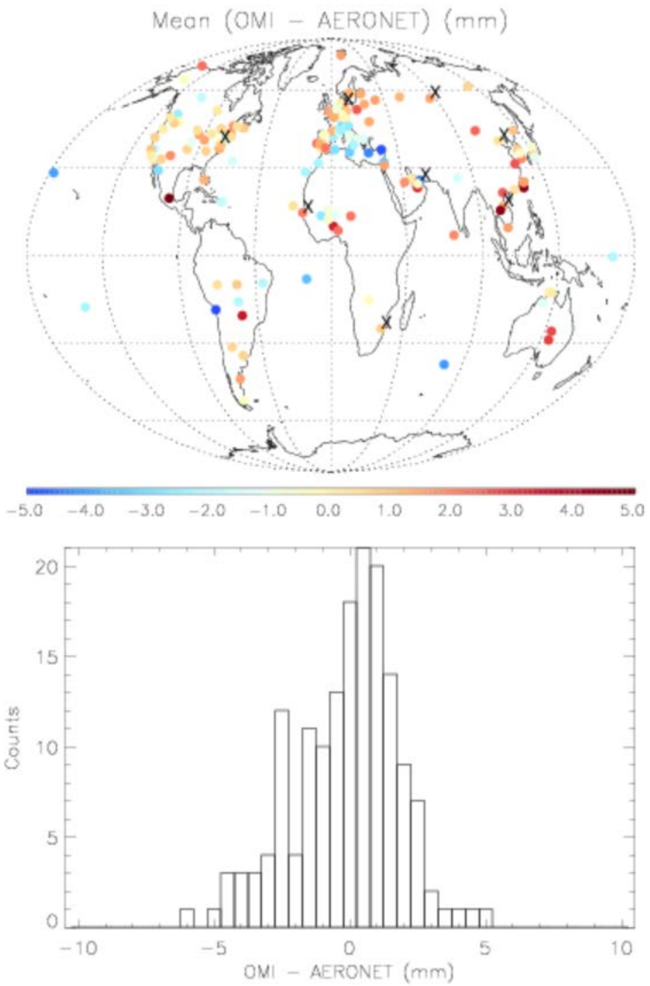

Figure 6. (Top) Spatial distribution of the time mean of (OMI – AERONET) from 2005 to 2009 at AERONET stations. (Bottom) Histogram (with a 0.5 mm bin size) for the values shown in the top panel.

Atmos. Chem. Phys. Discuss., doi:10.5194/acp-2016-181, 2016
Manuscript under review for journal Atmos. Chem. Phys.
Published: 18 April 2016

Atmospheric Chemistry and Physics
Discussions

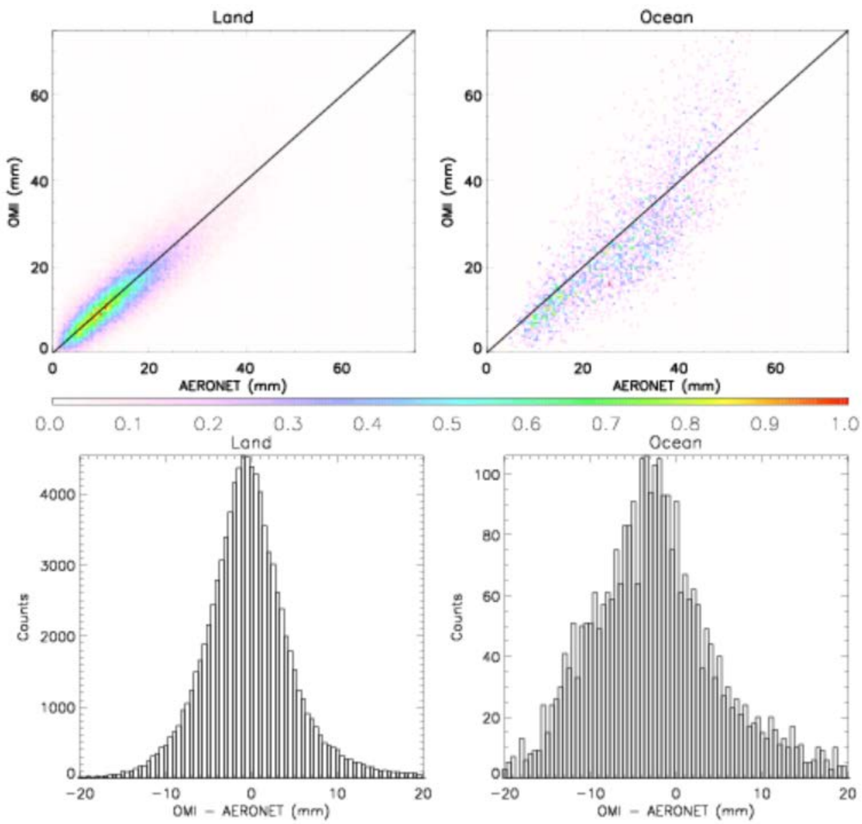

Figure 7. (Top) 2D normalized histogram for (left) land and (ocean) derived from all the paired OMI and AERONET data at all suitable AERONET stations from January 1, 2005 to December 31, 2009. Results are shown for 0.5 mm × 0.5 mm bins, with the largest binned value normalized to 1. The black line in each panel corresponds to 1:1. (Bottom) Histogram of (OMI – AERONET) derived from the same data as those used in the top panel. The counts correspond to 0.5 mm bins.

Atmos. Chem. Phys. Discuss., doi:10.5194/acp-2016-181, 2016
Manuscript under review for journal Atmos. Chem. Phys.
Published: 18 April 2016

Atmospheric Chemistry and Physics
Open Access
Discussions

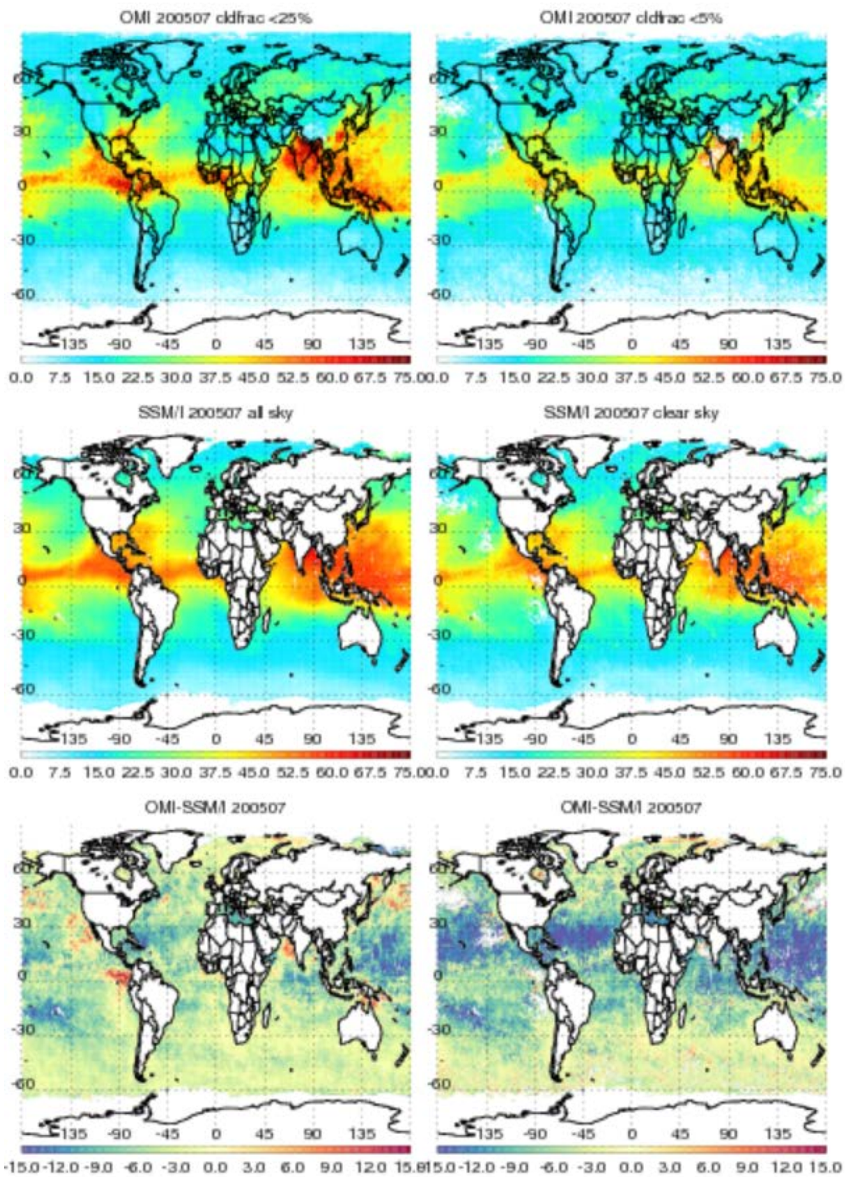

Figure 8. Monthly mean TCWV for July 2005 derived from (top left) OMI with a cloud fraction cutoff of 25%, (top right) OMI with a cloud fraction cutoff of 5%, (middle left) SSM/I under "all-sky" condition, and (middle right) SSM/I under "clear" sky condition. The bottom row shows the results of (top row - middle row).

Atmos. Chem. Phys. Discuss., doi:10.5194/acp-2016-181, 2016
Manuscript under review for journal Atmos. Chem. Phys.
Published: 18 April 2016

Atmospheric Chemistry and Physics
Open Access
Discussions

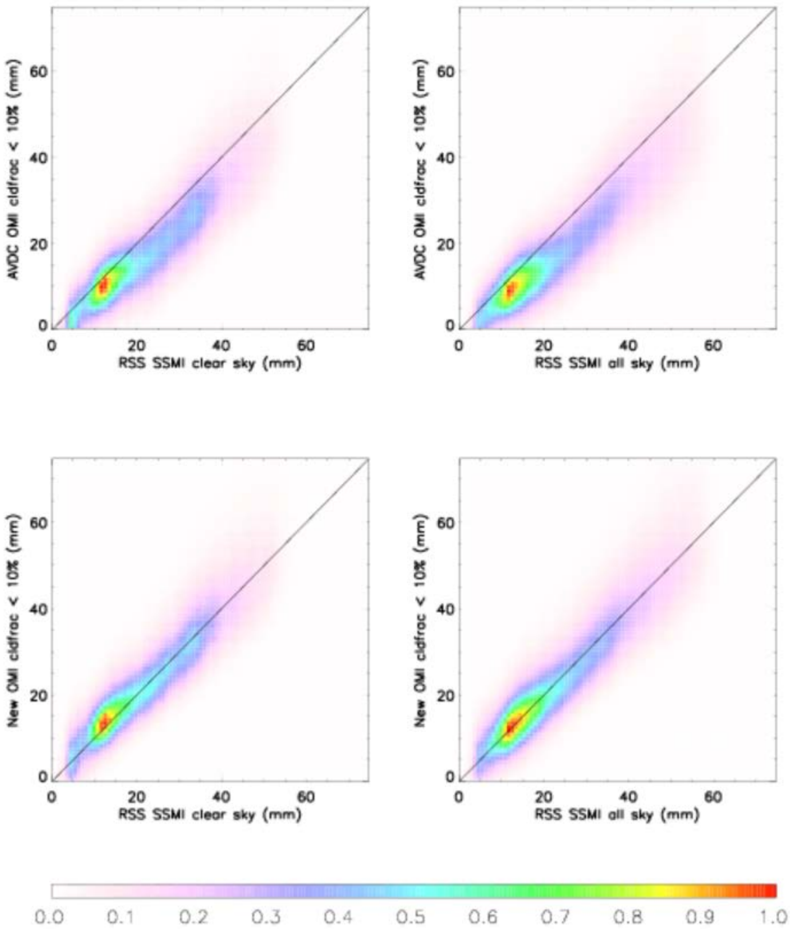

Figure 9. Two-dimensional normalized histograms derived from the daily gridded (0.5° × 0.5°) OMI and SSM/I data in July 2005 using 0.5 mm × 0.5 mm bins. The horizontal axes of the left column represent RSS SSM/I data for “clear” sky condition. The horizontal axes of the right column represent RSS SSM/I data for all-sky conditions. The vertical axes for the top row represent AVDC Collection 3 OMI data (generated with algorithm Version 1.0.0) with a cloud fraction cutoff of 10%. The vertical axes for the bottom row represent the OMI data generated with the new algorithm with a cloud fraction cutoff of 10%. The black line in each panel corresponds to 1:1.

Atmos. Chem. Phys. Discuss., doi:10.5194/acp-2016-181, 2016
Manuscript under review for journal Atmos. Chem. Phys.
Published: 18 April 2016

Atmospheric Chemistry and Physics
Discussions
Open Access

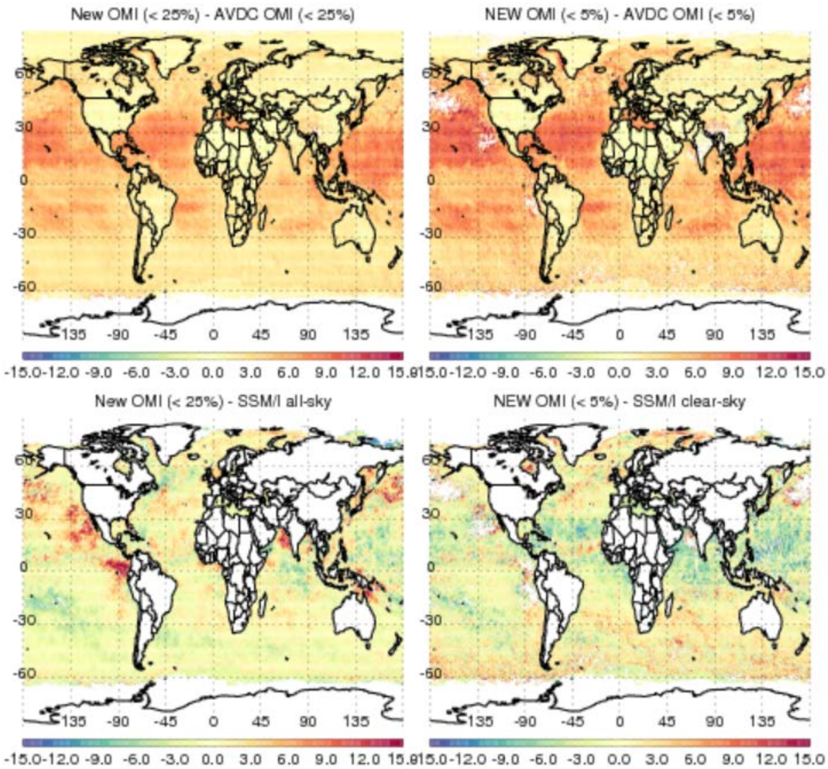

Figure 10. The top row shows the monthly mean difference of new OMI – AVDC Collection 3 OMI for July 2005. The top left panel uses a cloud fraction cutoff of 25% and the top right panel uses a cloud fraction cutoff of 5%. The bottom row shows the monthly mean difference of (new OMI – SSM/I). The bottom left panel corresponds to new OMI with a cloud fraction cutoff of 25% and SSM/I under all-sky conditions. The bottom right panel corresponds to new OMI with a cloud fraction cutoff of 5% and SSM/I under "clear" sky condition.